

1

[ATLAS Semivisible Jets]

2

[Elena Laura Busch]

3

Submitted in partial fulfillment of the
requirements for the degree of
Doctor of Philosophy
under the Executive Committee
of the Graduate School of Arts and Sciences

4

5

6

7

8

COLUMBIA UNIVERSITY

9

2024

10

© 2024

11

[Elena Laura Busch]

12

All Rights Reserved

13

Abstract

14

[ATLAS Semivisible Jets]

15

[Elena Laura Busch]

16

Abstract of dissertation (place-holder).

Table of Contents

18	Acknowledgments	v
19	Dedication	vi
20	Introduction or Preface	1
21	Chapter 1: The Standard Model	2
22	Chapter 2: The Large Hadron Collider	4
23	2.1 Accelerator Physics	5
24	2.1.1 The Journey of a Proton	5
25	2.1.2 Magnets	6
26	2.2 Luminosity	7
27	2.3 LHC Timeline	10
28	Chapter 3: The ATLAS Detector	12
29	3.1 Coordinate System and Geometry	12
30	3.2 Inner Detector	14
31	3.2.1 Pixel Detector	14
32	3.2.2 Semiconductor Tracker	15
33	3.2.3 Transition Radiation Tracker	15

34	3.3 Calorimeters	16
35	3.3.1 Liquid Argon Calorimeter	17
36	3.3.2 Tile Calorimeter	20
37	3.4 Muon Spectrometer	21
38	3.5 Magnet System	23
39	3.6 Forward Detectors	24
40	3.7 Trigger and Data Acquisition	25
41	Chapter 4: Particle Reconstruction and Identification	27
42	Conclusion or Epilogue	28
43	References	32
44	Appendix A: Experimental Equipment	34
45	Appendix B: Data Processing	35

List of Figures

47	2.1	The LHC accelerator complex at CERN [8]	6
48	2.2	The octants of the LHC and location of various beam activities [7]. Stars indicate the locations of beam collisions, and the associated detectors recording the outcome of those collisions.	7
51	2.3	(Left) Total integrated luminosity over the course of Run 2. (Right) Average number of pp interactions per bunch crossing in Run 2. Each curve is weighted by the integrated luminosity for the year.	9
54	2.4	Timeline of LHC and HL-LHC activities [10]. Integrated luminosity estimates are approximate, and not reflective of the exact amount delivered to each experiment.	11
56	3.1	ATLAS coordinate system and geometry	14
57	3.2	A 3D visualization of the structure of the ID in the barrel region [14]	15
58	3.3	ATLAS calorimetery system [15]	16
59	3.4	Diagram of a segment of the EMB, demonstrating the accordion plate arrangement [16]	18
61	3.5	A LAr pulse as produced in the detector (triangle) and after shaping (curve) [16] . .	19
62	3.6	Readout gap structure in HEC [16]	19
63	3.7	TileCal wedge module [19]	21
64	3.8	Cross section view of the muon spectrometer system [20]	22
65	3.9	Layout of the barrel and endcap toroid magnets [13]	24

List of Tables

67

Acknowledgements

68 Insert your acknowledgements text here. This page is optional, you may delete it if not
69 needed.

70

Dedication

71

Dedicated to my friends and family

72

Introduction or Preface

73 Insert your preface text here if applicable. This page is optional, you may delete it if not
74 needed. If you delete this page make sure to move page counter comment in thesis.tex to correct
75 location.

Chapter 1: The Standard Model

78 Four fundamental forces

79 The Standard Model is a universally accepted framework which explains most of the interactions of fundamental particles. The SM is a renormalizable quantum field theory that obeys the local symmetry G_{SM} :

$$G_{SM} = SU(3)_C \times SU(2)_L \times U(1)_Y \quad (1.1)$$

82 The $SU(3)_C$ symmetry component is the non-Abelian gauge group of quantum chromodynamics (QCD), the theory of strong interactions. There are 8 generators for the $SU_C(3)$ group which correspond to *gluons*, massless spin-1 gauge boson which carry the force of the strong interaction.

85 Gluon and quarks, the particles which interact with the strong force, carry a color charge C .

86 The $SU(2)_L \times U(1)_Y$ symmetry group represents the electroweak sector of the Standard Model. There are 4 generators for this group, which correspond to the four massless gauge bosons W^1 , W^2 , W^3 , and B. From these massless gauge bosons are formed the massive mediators of the weak force, the W^- , W^+ and Z^0 bosons, and the massless electromagnetic force carrier, the photon γ .

90 The interplay between the fermionic and bosonic fields that emerge from the G_{SM} symmetry can be described through the Lagrangian in equation 1.2

$$\mathcal{L} = \mathcal{L}_{kin} + \mathcal{L}_\psi + \mathcal{L}_{Yuk} + \mathcal{L}_\phi \quad (1.2)$$

92 Each term in this Lagrangian describes a set of specific particle physics interactions. \mathcal{L}_{kin} . with three families of quarks and leptons, and a scalar Higgs doublet. The standard model has 12 gauge bosons: 8 gluons, 3 weak bosons, and the photon. [1]

95 The physics of the Standard Model of particle physics (SM) is summarized by the SM Lagrangian:

$$\mathcal{L}_{kin} = -\frac{1}{4}F_{\mu\nu}F^{\mu\nu} \quad (1.3)$$

97 Explain equation

98 Explain phenomonolyg

Chapter 2: The Large Hadron Collider

101 The Large Hadron Collider (LHC) is a 26.7 km circular high-energy particle accelerator, span-
102 ning the Swiss-French border near the city of Geneva, Switzerland [2]. The LHC occupies the
103 tunnel constructed in 1989 for the Large Electron-Positron (LEP) Collider, and reaches a maxi-
104 mum depth of 170m below the surface. The LHC is operated by the European Organization for
105 Nuclear Research (CERN), the largest international scientific collaboration in the world.

106 The LHC accelerates protons and heavy ions, and collides them at four interaction points
107 around the ring, with a design center-of-mass energy per collision of $\sqrt{s} = 14$ TeV. Each interaction
108 point is home to one of four detector experiments, which study the products of the collisions. The
109 largest of these experiments is the ATLAS detector, a general purpose detector designed to study
110 the Standard Model and search for new physics that could be produced in LHC collisions [3]. The
111 CMS detector is another general purpose detector, designed and operated independently of the AT-
112 LAS detector, but intended to probe the same range of physics [4]. The ALICE experiment is a
113 dedicated heavy ion experiment, and the LHC-b experiment is a dedicated *b*-physics experiment
114 [5] [6].

115 This chapter will cover the multi-component accelerator complex powering the LHC, the state-
116 of-the-art magnets which steer the particle beams, measurements of the intensity and number of
117 collisions produced by the LHC, and finally an overview of LHC activities in the past, present, and
118 future.

¹¹⁹ **2.1 Accelerator Physics**

¹²⁰ **2.1.1 The Journey of a Proton**

¹²¹ From 2010 - 2018, the protons which fed the LHC started as hydrogen gas. The electrons were
¹²² removed from the hydrogen atoms through the use of strong electric fields. The linear accelerator
¹²³ LINAC2 then accelerated the protons to an energy of 50 MeV. Between 2018 and 2020, LINAC2
¹²⁴ was replaced with LINAC4, which instead accelerates H^- ions, hydrogen atoms with two electrons.
¹²⁵ LINAC4 is capable of accelerating the H^- ions to 160 MeV. Before injection to the next part of
¹²⁶ the acceleration chain, both electrons are stripped from the H^- ions, leaving just protons. From
¹²⁷ here the protons enter the Proton Synchrotron booster, where they are accelerated up to 1.4 GeV of
¹²⁸ energy. Subsequently they are sorted into bunches separated in time by 25 ns, where each bunch
¹²⁹ contains approximately 10^{11} protons. Next the bunches pass through the Proton Synchrotron (PS)
¹³⁰ and the Super Proton Synchrotron (SPS), where they reach energies of 25 GeV and 450 GeV
¹³¹ respectively. Finally they are injected into the LHC as two beams traveling in opposite direction.
¹³² The original design allowed each beam to be accelerated up to 7 TeV of energy. Due to limitations
¹³³ in the performance of the superconducting LHC magnets, the highest energy actually achieved by
¹³⁴ the LHC beams during Run 2 was 6.5 TeV, giving a collision center-of-mass energy of $\sqrt{s} = 13$
¹³⁵ TeV [7]. Figure 2.1 shows the full LHC accelerator complex.

¹³⁶ Acceleration in the LHC is performed by eight radio frequency (RF) cavities located around the
¹³⁷ ring. Each RF cavity produces a 2 MV electric field oscillating at 40 MHz. The 40MHz oscillation
¹³⁸ produces a point of stable equilibrium every 2.5 ns. These points of equilibrium are synchronized
¹³⁹ with the occurrence of the proton bunches produced in the PS – a proton bunch occupies one out
¹⁴⁰ of every ten points of stable equilibrium, such that the bunches maintain a 25 ns spacing [7].

¹⁴¹

The CERN accelerator complex Complexe des accélérateurs du CERN

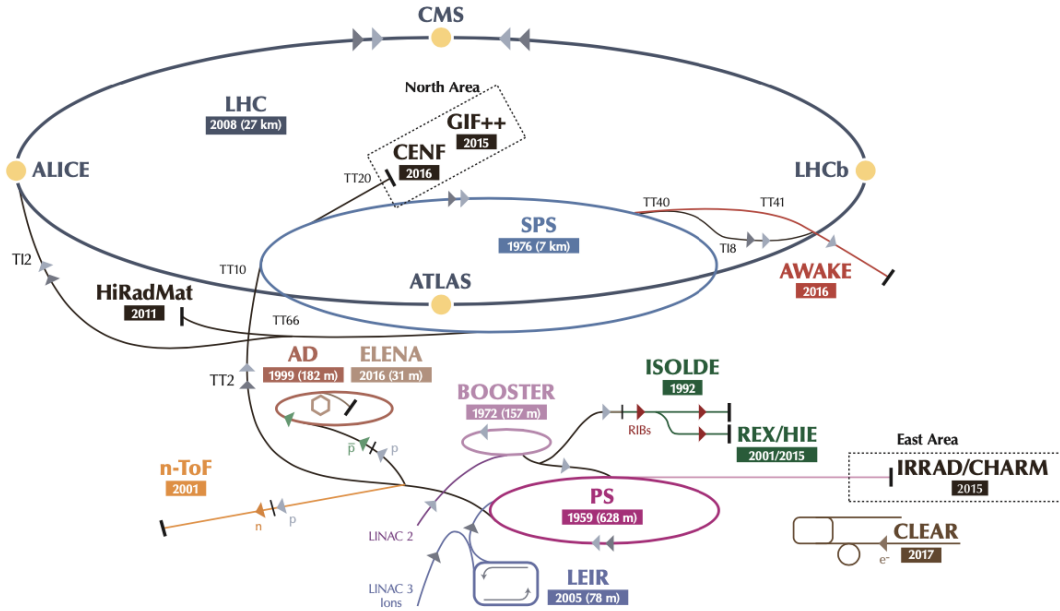


Figure 2.1: The LHC accelerator complex at CERN [8]

¹⁴² 2.1.2 Magnets

¹⁴³ In addition to the acceleration cavities, the LHC houses 9593 superconducting magnets which
¹⁴⁴ direct and focus the proton beam on its 27 kilometer journey. The magnets are comprised of super-
¹⁴⁵ conducting Niobium-Titanium coils cooled to 1.9K by superfluid helium. As the beams approach
¹⁴⁶ one of the four collision points around the ring, multipole magnets focus and squeeze the beam for
¹⁴⁷ optimal collisions [7].

¹⁴⁸ The LHC is divided into sections, where each section contains an arc and a straight insertion. The arcs are composed of 1232 large dipole magnets which bend the beam
¹⁴⁹ to follow the roughly circular 27 km path. The main dipoles generate powerful 8.3 tesla magnetic
¹⁵⁰ fields to achieve this bend. Each dipole magnet is 15 meters long and weighs 35 tonnes. The
¹⁵¹ dipoles work in conjunction with quadrupole magnets, which keep the particles in a focused beam,
¹⁵² and smaller sextupole, octupole and decapole magnets which tune the magnetic field at the ends of
¹⁵³ the dipole magnets [9].

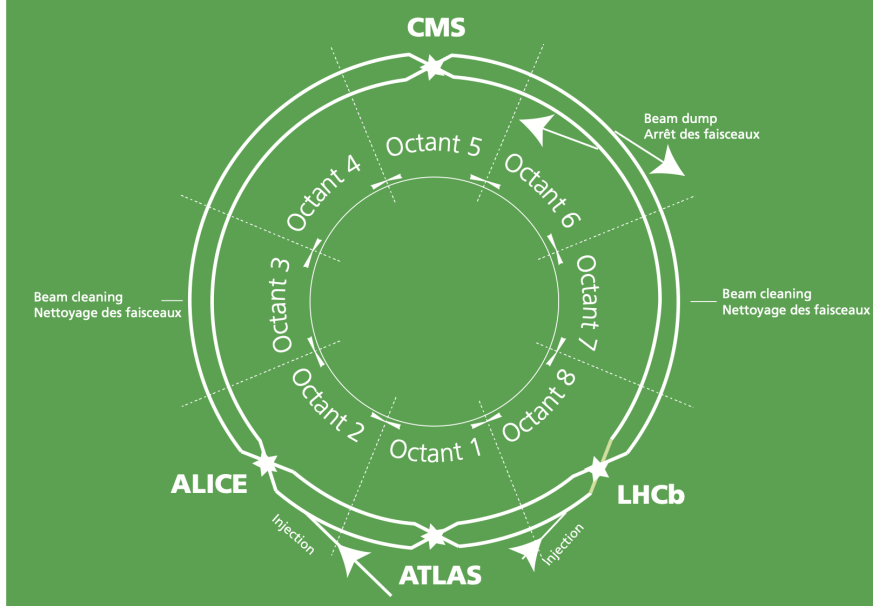


Figure 2.2: The octants of the LHC and location of various beam activities [7]. Stars indicate the locations of beam collisions, and the associated detectors recording the outcome of those collisions.

155 The straight insertion sections have different purposes depending on their location around the
 156 ring: beam collisions, beam injection, beam dumping, or beam cleaning. At the four collision
 157 points, insertion magnets squeeze the beam to ensure a highly focused collision. This is accom-
 158 plished with a triplet of quadrupole magnets, which tighten the beam from 0.2 millimeters to just
 159 16 micrometers in diameter. Insertion magnets also clean the beam, which prevents stray particles
 160 from hitting sensitive components throughout the LHC. When the LHC is ready to dispose of a
 161 beam of particles, beam dump magnets deflect the path of the beam into a straight line towards
 162 a block of concrete and graphite that stops the beam. A dilution magnet then reduces the beam
 163 intensity by a factor of 100,000 before the final stop [9]. Figure 2.2 shows the locations various
 164 beam activities.

165 **2.2 Luminosity**

166 Collisions at the LHC occur when the two beams of proton bunches cross at one of the four
 167 interaction points. The intensity of collisions is described by the instantaneous luminosity, the

168 formula for which is given in equation 2.1.

$$L = \frac{fN_1N_2}{4\pi\sigma_x\sigma_y} \quad (2.1)$$

169 Here f is the revolution frequency, N_1 and N_2 are the number of particle per bunch for each
170 beam, and σ_x , σ_y are the horizontal and vertical beam widths.

171 The instantaneous luminosity gives the number of the collisions that could be produced at the
172 interaction point per unit of cross-sectional area per unit of time, generally expressed in $\text{cm}^{-2}\text{s}^{-1}$.
173 The integrated luminosity is obtained by integrating the instantaneous luminosity over a given
174 block of time, and measures the total number of collisions which have occurred during that op-
175 eration period. The total integrated luminosity is directly correlated with the size of the datasets
176 collected by the LHC experiments. Total integrated luminosity for Run 2 is illustrated in Figure
177 2.3.

178 High levels of instantaneous luminosity result in multiple pp collisions per bunch crossing,
179 which leads to an effect known as *pileup*. Pileup poses a challenge for detector physics, as recon-
180 structing the products of multiple simultaneous events is far more challenging than reconstructing
181 a single event with no pileup. Pileup conditions vary from year-to-year and run-to-run of LHC op-
182 eration, and the impact of these conditions are taken into account when analyzing the data, as will
183 be discussed further in Chapter 4. Measurement of pileup conditions during Run 2 are illustrated
184 in Figure 2.3.

185 The design peak luminosity of the LHC is $1.0 \times 10^{34} \text{ cm}^{-2}\text{s}^{-1}$. During Run 1 of the LHC the
186 peak instantaneous luminosity was $0.8 \times 10^{34} \text{ cm}^{-2}\text{s}^{-1}$. Over the course of Run 1 the LHC collected
187 a total integrated luminosity of 5.46 fb^{-1} at $\sqrt{s} = 7 \text{ TeV}$, and 22.8 fb^{-1} at $\sqrt{s} = 8 \text{ TeV}$. Following the
188 first long shutdown and upgrade phase of operations, the LHC achieved a center of mass energy
189 $\sqrt{s} = 13 \text{ TeV}$ at the beginning of Run 2 in 2015. The LHC was also able to deliver 2.0×10^{34}
190 $\text{cm}^{-2}\text{s}^{-1}$ peak instantaneous luminosity, double the design value. During LHC Run 2, from 2015-
191 2018, the LHC delivered 156 fb^{-1} of integrated luminosity for proton-proton collisions. Run 3 of

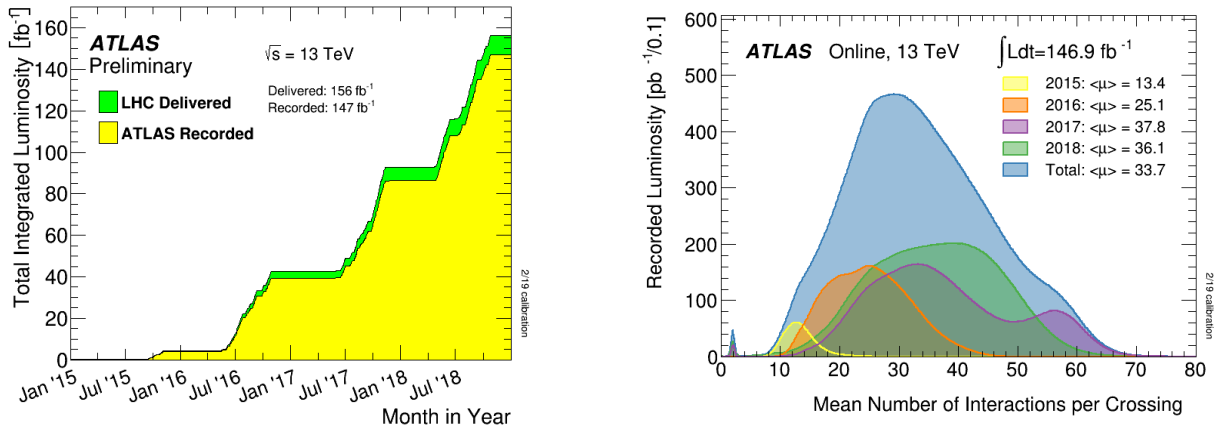


Figure 2.3: (Left) Total integrated luminosity over the course of Run 2. (Right) Average number of pp interactions per bunch crossing in Run 2. Each curve is weighted by the integrated luminosity for the year.

192 the LHC began in 2022, and is expected to deliver 250 fb^{-1} of integrated luminosity to the ATLAS
193 and CMS experiments by 2026 [10].

194 The goal of LHC physic analyses is to find and study rare events produced by interesting
195 physics processes. The cross section σ of a given process indicates the probability of that process
196 occurring given the beam conditions of the LHC. Multiplying the cross section by the integrated
197 luminosity of a dataset gives the expected number of events for that process within the dataset.

$$N_{\text{events}} = \int \sigma L(t) dt = \mathcal{L} \times \sigma \quad (2.2)$$

198 The cross section for most processes of interest, especially BSM processes, is several orders of
199 magnitude below the total cross section for the LHC. Therefore maximizing the number of events
200 produced in collisions is crucial to increase the likelihood of producing events from processes of
201 interest. For this reason, maximizing instantaneous luminosity is a key factor in accelerator design
202 and operation, while mitigating the resulting pileup effects is a key component in detector design
203 and operation.

204 **2.3 LHC Timeline**

205 The first proton-proton collisions at the LHC were achieved in 2010 with a center-of-mass
206 energy of $\sqrt{s} = 7$ TeV. Run 1 of the LHC took place between 2010 and early 2013, during which
207 time the center-of-mass collision energy increased from 7 TeV to 8 TeV. Figure 2.4 shows an
208 overview of LHC activities beginning in 2011, in the midst of Run 1. The data collected during
209 Run 1 led to the discovery of the Higgs Boston in 2012 [11].

210 Between 2013 and 2015 the LHC underwent the first Long Shutdown (LS1) during which
211 time maintenance and renovation was performed on the accelerator chain, including the repair and
212 consolidation of the high-current splices which connect the super-conducting LHC magnets. Run
213 2 of the LHC took place from 2015 to 2018 and achieved a center-of-mass energy of $\sqrt{s} = 13$ TeV.
214 Analysis of data collected in Run 2 is still on going, and is the subject of study in this thesis.

215 Between 2018 and 2022 the LHC underwent the second Long Shutdown (LS2), allowing for
216 further detector and accelerator maintenance and upgrades. Key improvements to the LHC in-
217 cluded the improvement of the insulation for over 1200 diode magnets, and the upgrade from
218 LINAC2 to LINAC4 mentioned in Section 2.1.1. Run 3 of the LHC began in 2022 and achieved a
219 center-of-mass energy of $\sqrt{s} = 13.6$ TeV.

220 Run 3 is scheduled to continue through 2026, at which point the LHC machine and detectors
221 will undergo upgrades for the *high luminosity* LHC (HL-LHC). The HL-LHC will increase the
222 instantaneous machine luminosity by a factor of 5 - 7.5 with respect to the nominal LHC design.
223 The bottom panel of Figure 2.4 shows an overview of the preparation work for the HL-LHC that
224 has been going on concurrently with Run 1, 2, and 3 of the LHC [12].



Figure 2.4: Timeline of LHC and HL-LHC activities [10]. Integrated luminosity estimates are approximate, and not reflective of the exact amount delivered to each experiment.

225

226

Chapter 3: The ATLAS Detector

227 The ATLAS detector (**A Toroidal LHC ApparatuS**) is one of two general purpose physics
228 detectors designed to study the products of proton-proton collisions at the LHC. The detector is
229 composed of a variety of specialized subsystems, designed to fully capture a wide array of physics
230 processes. The apparatus is 25m high, 44m in length, and weighs over 7000 tons [13]. The LHC
231 beam pipes direct proton beams to an interaction point at the center of ATLAS, and the cylindrical
232 detector design captures a complete 360° view of the *event*, tracking all particles that result from
233 the collision.

234 The main components of the ATLAS detector are the Inner Detector (ID) which provides high
235 precision tracking of charged particles leaving the collision vertex, the calorimeter system which
236 measures the energy of electromagnetic and hadronic objects, and the Muon Spectrometer (MS)
237 which gives detailed information about muons that reach the outer radii of the detector. Two
238 magnet systems, a 2 T solenoid magnet surrounding the ID, and a 0.5-1.0 T toroid magnet system
239 situated throughout the MS, produce magnetic fields which bend the trajectory of charged particles
240 traversing the detector. In addition to the main detector components, dedicated forward detectors
241 monitor beam conditions and instantaneous luminosity, and an online trigger system reduces the
242 data rate to a manageable level for storage. Each of these components will be discussed in further
243 detail in this chapter.

244 **3.1 Coordinate System and Geometry**

245 The ATLAS detector employs a right hand cylindrical coordinate system. The z axis is aligned
246 with the beam line, and the x-y plane sits perpendicular to the beam line. The coordinate system
247 origin is centered on the detector, such that the origin corresponds with the interaction point of the

248 two colliding beams. The detector geometry is usually characterized by polar coordinates, where
249 the azimuthal angle ϕ spans the x-y plane. The polar angle θ represents the angle away from the
250 beam line, or z axis. $\theta = 0$ aligns with the positive z -axis, and $\phi = 0$ aligns with the positive x-axis.

251 The polar coordinate θ is generally replaced by the Lorentz invariant quantity *rapidity* or y :

$$y = \frac{1}{2} \ln\left(\frac{E + p_z}{E - p_z}\right). \quad (3.1)$$

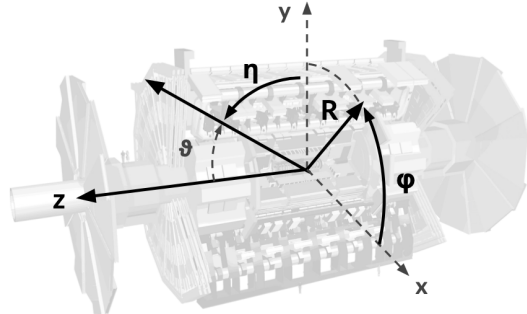
252 This substitution is advantageous because objects in the detector are traveling at highly rela-
253 tivistic speeds. The relativistic speed also means that the masses of the particles are generally small
254 compared to their total energy. In the limit of zero mass, the rapidity y reduces to the pseudorapid-
255 ity η , which can be calculated directly from the polar angle θ :

$$\eta = -\ln\left(\frac{\theta}{2}\right). \quad (3.2)$$

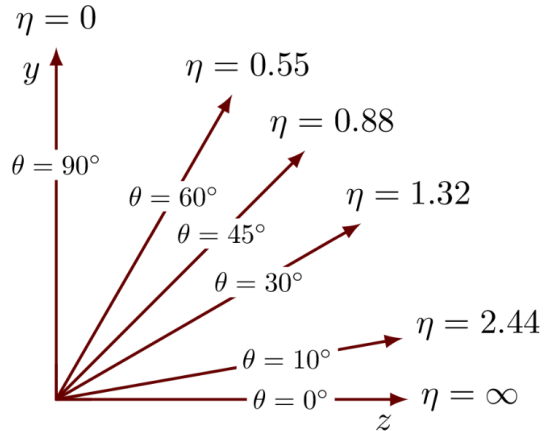
256 The distance between physics objects in the detector is generally expressed in terms of the solid
257 angle between them ΔR :

$$\Delta R = \sqrt{\Delta\phi^2 + \Delta\eta^2} \quad (3.3)$$

258 Figure 3.1a depicts the orientation of the coordinate system with respect to the ATLAS detector,
259 while Figure 3.1b illustrates the relationship between θ , η , and the beamline axis z . Direct or “head
260 on” proton-proton collisions are more likely to result in objects whose momentum is directed
261 along transverse plane (low $|\eta|$); glancing proton-proton collisions are more likely to result in
262 objects whose momentum is directed along the z -axis (high $|\eta|$). Due to the difference in the
263 nature of these collisions, as well as the cylindrical design of the ATLAS detector, the detector
264 is divided into regions of low and high η . Each subsystem has a “central” or “barrel” region
265 covering low $|\eta|$, while the “forward” or “end-cap” regions cover the area up to $|\eta| = 4.9$. Each of
266 the three main ATLAS subsystems will be discussed in the following sections.



(a) The ATLAS geometry



(b) Relationship between η and θ

Figure 3.1: ATLAS coordinate system and geometry

267 3.2 Inner Detector

268 The Inner Detector (ID) is the ATLAS subsystem closest to the interaction point. The primary
 269 purpose of the ID is to determine the charge, momentum, and trajectory of charged particles pass-
 270 ing through the detector. With this information the ID is also able to precisely determine interaction
 271 vertices.

272 The ID is composed of three sub-detectors; the Pixel Detector, the Semiconductor Tracker
 273 (SCT) and the Transition Radiation Tracker (TRT). Figure 3.2 shows the location of these three
 274 subsystems with respect to each other and the interaction point.

275 3.2.1 Pixel Detector

276 The pixel detector is the first detector encountered by particles produced in LHC collisions.
 277 The original pixel detector consists of 3 barrel layers of silicon pixels, positioned at 5 cm, 9 cm
 278 and 12 cm from the beamline. There are also 3 disks on each end-cap positioned 50 - 65 cm from
 279 the interaction point, providing full coverage for $|\eta| < 2.2$. The layers are comprised of silicon
 280 pixels each measuring $50 \times 400 \mu\text{m}^2$, with 140 million pixels in total. The pixels are organized
 281 into modules, which each contain a set of radiation hard readout electronics chips. In 2014, the
 282 Insertable B-layer (IBL) was installed, creating a new innermost layer of the pixel detector sitting

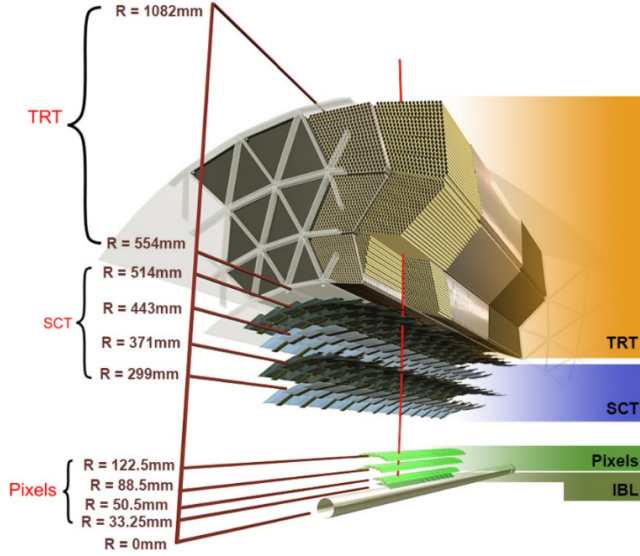


Figure 3.2: A 3D visualization of the structure of the ID in the barrel region [14]

just 3.3 cm from the beamline. The pixels of the IBL measure $50 \mu\text{m}$ by $250 \mu\text{m}$, and cover a pseudo-rapidity range up to $|\eta| < 3$. The IBL upgrade enhances the pixel detector's ability to reconstruct secondary vertices associated with short-lived particles such as the b-quark. The improved vertex identification also helped compensate for increasing pile-up in Run 2 [13].

3.2.2 Semiconductor Tracker

The SCT provides at least 4 additional measurements of each charged particle. It employs the same silicon technology as the Pixel Detector, but utilizes larger silicon strips which measure $80 \mu\text{m}$ by 12.4 cm . The SCT is composed of 4 barrel layers, located between 30 cm and 52 cm from the beamline, and 9 end-cap layers on each side. The SCT can distinguish tracks that are separated by at least $200 \mu\text{m}$.

3.2.3 Transition Radiation Tracker

The TRT provides an additional 36 hits per particle track. The detector relies on gas filled straw tubes, a technology which is intrinsically radiation hard. The straws which are each 4 mm in diameter and up to 150 cm in length and filled with xenon gas. The detector is composed of about

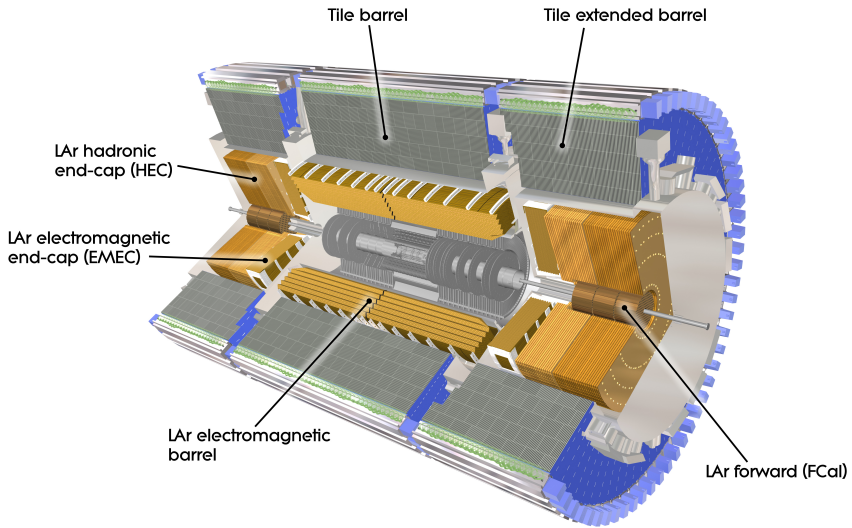


Figure 3.3: ATLAS calorimetry system [15]

297 50000 barrel region straws and 640000 end-cap straws, comprising 420000 electronic readout
 298 channels. Each channel provides a drift time measurement with a spatial resolution of $170\text{ }\mu\text{m}$ per
 299 straw. As charged particles pass through the many layers of the detector, transition radiation is
 300 emitted. The use of two different drift time thresholds allows the detector to distinguish between
 301 tracking hits and transition radiation hits.

302 3.3 Calorimeters

303 The ATLAS calorimeter system is responsible for measuring the energy of electromagnetically
 304 interacting and hadronically interacting particles passing through the detector. The calorimeters are
 305 located just outside the central solenoid magnet, which encloses the inner detectors. The calorime-
 306 ters also stop most known particles, which the exception of muons and neutrinos, preventing them
 307 from traveling to the outermost layers of the detector. The ATLAS calorimetry system is composed
 308 of two subsystems - the Liquid Argon (LAr) calorimeter for electromagnetic calorimetry and the
 309 Tile calorimeter for hadronic calorimetry. The full calorimetry system is shown in Figure 3.3.

310 3.3.1 Liquid Argon Calorimeter

311 The LAr calorimeter is a sampling calorimeter designed to trigger on and measure the ener-
312 gies of electromagnetic (EM) particles, as well as hadronic particles in the high η regions. It is
313 divided in several regions, as shown in Figure 3.3. For the region $|\eta| < 1.4$, the electromagnetic
314 barrel (EMB) is responsible for EM calorimetry, and provides high resolution energy, timing,
315 and position measurements for electrons and photons passing through the detector. The elec-
316 tromagnetic endcap (EMEC) provides additional EM calorimetry up to $|\eta| < 3.2$. In the re-
317 gion $1.4 < |\eta| < 3.2$, the hadronic endcap (HEC) provides hadronic calorimetry. For hadronic
318 calorimetry in the region $|\eta| < 1.4$, corresponding to a detector radii > 2.2 m, the less expensive
319 tile calorimeter (discussed in the next section) is used instead. A forward calorimeter (FCAL)
320 extends the hadronic calorimetry coverage up to $3.1 < |\eta| < 4.8$ [16].

321 The LAr calorimeter is composed of liquid argon sandwiched between layers of absorber mate-
322 rial and electrodes. Liquid argon is advantageous as a calorimeter active medium due to its natural
323 abundance and low cost, chemical stability, radiation tolerance, and linear response over a large
324 energy range [17]. The calorimeter is cooled to 87k by three cryostats: one barrel cryostat encom-
325 passing the EMB, and two endcap cryostats. The barrel cryostat also encloses the solenoid which
326 produces the 2T magnetic field for the inner detector. Front-end electronics are housed outside the
327 cryostats and are used to process, temporarily store, and transfer the calorimeter signals.

328 **Electromagnetic Calorimeter**

329 For the electromagnetic calorimeters, the layers of electrodes and absorber materials are ar-
330 ranged in an an accordion shape, as illustrated in Figure 3.4. The accordion shape ensures that
331 each half barrel is continuous in the azimuthal angle, which is a key feature for ensuring consistent
332 high resolution measurements. Liquid argon permeates the space between the lead absorber plates,
333 and a multilayer copper-polymide readout board runs through the center of the liquid argon filled
334 gap.

335 The detection principle for the LAr calorimeter is the current created by electrons which are

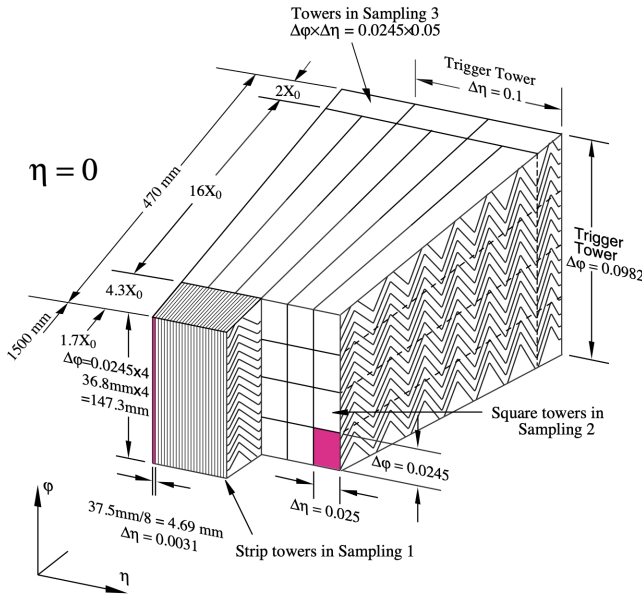


Figure 3.4: Diagram of a segment of the EMB, demonstrating the accordion plate arrangement [16]

336 released when a charged particle ionizes the liquid argon. In the barrel region, the electrons are
 337 driven towards the center electrodes by a 2000 V potential with a drift time of less than 450 ns [18].
 338 In the end-caps the voltage varies as a function of the radius in order to maintain a flat response
 339 [16]. The amount of current produced by the ionized electrons is proportional to the energy of
 340 the particle creating the signal. Figure 3.5 shows the shape of the signal produced in the LAr
 341 calorimeter, before and after it undergoes shaping during the readout process. The shaping of the
 342 pulse enforces a positive peak and a negative tail, which ensures that subsequence pulses can be
 343 separated with the precision required for the 25 ns LHC bunch spacing [16].

344 Hadronic End-cap Calorimeter

345 The HEC sits radially beyond the EMEC. The copper absorber plates in the HEC are oriented
 346 perpendicular to the beamline, with LAr as the active medium. Each end-cap is divided into two
 347 independent wheels; the inner wheel uses 25 mm copper plates, while the outer wheel uses 50 mm
 348 plates as a cost saving measure. In each wheel, the 8.5 mm plate gap is crossed by three parallel

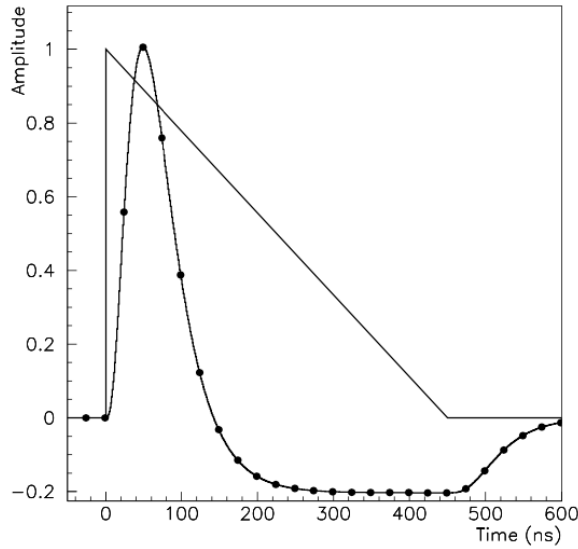


Figure 3.5: A LAr pulse as produced in the detector (triangle) and after shaping (curve) [16]

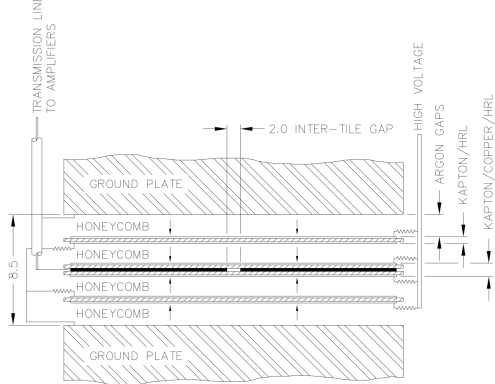


Figure 3.6: Readout gap structure in HEC [16]

349 electrodes, creating an effective drift distance of 1.8 mm. This gap is illustrated in Figure 3.6.
 350 Each wheel is divided into 32 wedge-shaped modules, each containing their own set of readout
 351 electronics.

352 **Forward Calorimeter**

353 The forward range is covered by the FCal, which provides both EM and hadronic calorimetry.
 354 It is composed of three active cylindrical modules; one EM module with copper absorber plates,
 355 and two hadronic modules with tungsten absorber plates. The plates are oriented perpendicular to

356 the beamline, and LAr is used as the active material throughout. The electrodes of the FCal consist
357 of tubes that run parallel to the beam line, arranged in a honeycomb pattern. The resulting LAr
358 gaps are as small as $250\ \mu\text{m}$, which enables the FCal to handle the large influx of particles in the
359 forward region [16].

360 3.3.2 Tile Calorimeter

361 The Tile Calorimeter (TileCal) provides hadronic calorimetry in the region $\eta < 1.7$, and sur-
362 rounds the LAr calorimeter. It is responsible for measurements of jet energy and jet substructure,
363 and also plays an important role in electron isolation and triggering (including muons) [19]. Tile-
364 Cal is composed of 3 sections, as shown in Figure 3.3; a barrel calorimeter sits directly outside the
365 LAr EMB and provides coverage up to $\eta < 1.0$. Two extended barrel sections sit outside the LAr
366 endcaps and cover the region $0.8 < \eta < 1.7$.

367 TileCal is a sampling calorimeter composed of steel and plastic scintillator plates as illustrated
368 in Figure 3.7. A total of 460,000 scintillators are read out by wavelength-shifting fibers. The
369 fibers are gathered to define cells and in turn read out by photomultiplier tubes, which amplify
370 the signal and convert it to an electrical signature. Each cell has an approximate granularity of
371 $\Delta\eta \times \Delta\phi = 0.1 \times 0.1$. Each barrel is divided azimuthally into 64 independent modules, an example
372 of which is show in Figure 3.7. The modules are each serviced by front-end electronic housed in a
373 water-cooled drawer on the exterior of the module.

374 The detection principle of the TileCal is the production of light from hadronic particles inter-
375 acting with the scintillating tiles. When a hadronic particle hits the steel plate, a shower of particles
376 are produced. The interaction of the shower with the plastic scintillator produces photons, the num-
377 ber and intensity of which are proportional to the original particle's energy.

378

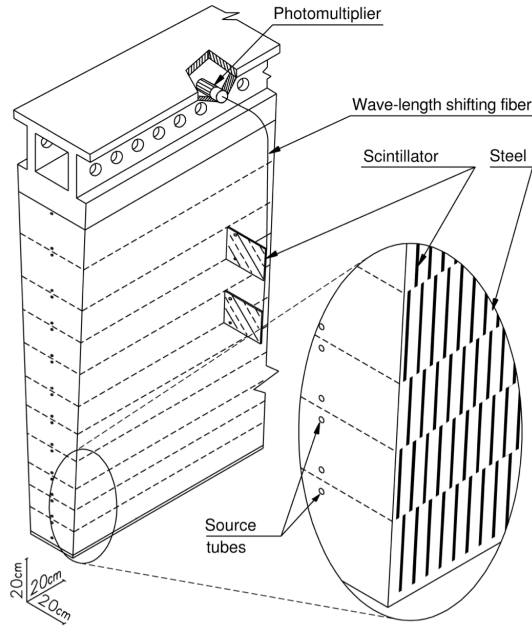


Figure 3.7: TileCal wedge module [19]

³⁷⁹ 3.4 Muon Spectrometer

³⁸⁰ Unlike electrons, photons, and hadrons, muons interact minimally with the ATLAS calorimeters, and can pass through large amounts of detector material without stopping. The ATLAS Muon ³⁸¹ Spectrometer (MS) provides additional tracking information to improve the identification and measurement ³⁸² of muons. The MS comprises the outermost layers of the detector, and is interspersed ³⁸³ with toroid magnets (discussed in Section 3.5), which provide a magnetic field of approximately ³⁸⁴ 0.5 T. The magnetic field bends the trajectory of the muons as they pass through the detector, and ³⁸⁵ the degree of the bend is directly correlated with the muon momentum. The path of the muon is ³⁸⁶ primarily measured by hits in three layers of Monitored Drift Tube (MDT) precision chambers, ³⁸⁷ which cover the range $|\eta| < 2.7$. The barrel layout of the MS is show in Figure 3.8. ³⁸⁸

³⁸⁹ Muon triggering is provided by three layers of Resistive Plate Chambers (RPC) in the barrel ³⁹⁰ ($|\eta| < 1.05$), and 3 - 4 layers of Thin Gap Chambers (TGC) in the end-caps ($1.05 < |\eta| < 2.4$). ³⁹¹ RPCs and TGCs also provide muon track measurements in the non-bending coordinate (ϕ). RPCs ³⁹² are constructed from two parallel resistive plates separated by a 2mm gap filled with a sensitive

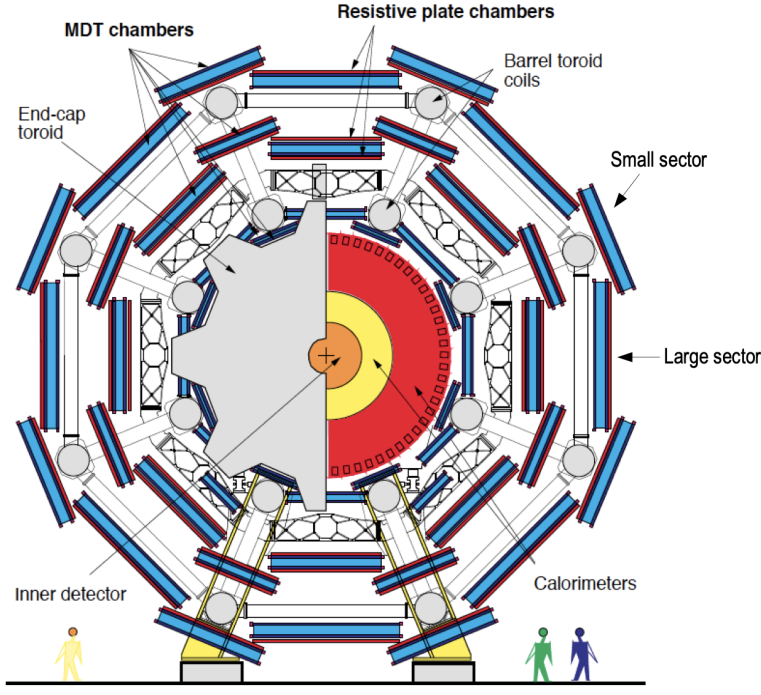


Figure 3.8: Cross section view of the muon spectrometer system [20]

393 gas mixture. This provides a total of six independent measurements for each muon track, with a
 394 spatial resolution of ~ 1 cm and a time resolution of ~ 1 ns. Time measurements from the RPCs
 395 are primarily associated to hits in the MDT precision chambers to determine the bunch crossing.
 396 The time measurement is also used to reject cosmic muons, and to search for delayed signals.
 397 TCGs provide triggering in the end-cap regions, and consist of parallel $30\ \mu\text{m}$ wires suspended
 398 in a sensitive gas mixture. TCGs provide high radiation tolerance and a fast response time, both
 399 features that are necessary for handling the high flux of muons in the forward region [20].

400 Precision measurements of muon momentum and position are primarily achieved by MDTs.
 401 The MDTs are constructed from 30 mm diameter tubes, permeated by a gas mixture of 93% Ar and
 402 7% CO₂. The average single-tube spatial resolution is $80\ \mu\text{m}$. Each chamber consists of six drift
 403 tube layers, which together provide a muon track segment resolution of $35\ \mu\text{m}$. The momentum
 404 of the muons can be calculated from the bend in the muon trajectory as they pass through the
 405 0.5T magnetic field provided by the toroids. For a $p_T = 1$ TeV track, the average p_T resolution is
 406 11%. In the inner most end-cap wheels, Cathode Strip Chambers (CSC) are used instead of MDTs,

407 covering the region $2.0 < |\eta| < 2.7$. CSCs are multi-wire proportional chambers, with a cathode
408 strip readout. The CSCs have a spatial resolution in the range of $50 \mu\text{m}$, and a maximum drift time
409 of about 30 ns, which makes them superior for handling the high flux of particles in the forward
410 region [21].

411 **3.5 Magnet System**

412 The ATLAS magnet system consists of four sets of superconducting magnets: a barrel solenoid,
413 a barrel toroid, and two end-cap toroids. The solenoid magnet produces a 2T magnetic field re-
414 sponsible for bending the trajectories of charged particles as they pass through the inner detector.
415 The three toroid magnets provide a field of 0.5 - 1 T and curve the path of muons passing through
416 the muon spectrometer.

417 The inner solenoid magnet is composed of over 9 km of niobium-titanium superconductor
418 wires, which are imbedded into strengthen pure aluminum strips. The solenoid is just 4.5 cm
419 thick, which minimizes interactions between the magnet material and particles passing through the
420 detector. It is housed in the LAr cryostat, as described in section 3.3.1, which further reduces the
421 amount of non-detector material required to support the solenoid. The return yoke of the magnet
422 is provided by the iron absorber of the TileCal [22].

423 The central ATLAS toroid magnet, providing the magnetic field for the barrel region of the MS,
424 is the largest toroidal magnet ever constructed at 25 m in length. The toroid is composed of eight
425 individual coils, each housed in their own cryostat. The toroidal magnetic field is advantageous
426 as the direction of the field is almost perpendicular to the path of the charged particles. 56 km of
427 aluminum stabilized niobium-titanium-copper superconductor wire compose the magnet. In each
428 end-cap, eight smaller superconducting coils extend the toroidal magnetic field to particles leaving
429 the detector in the forward direction [22]. Figure 3.9 shows the layout of the toroid magnets.

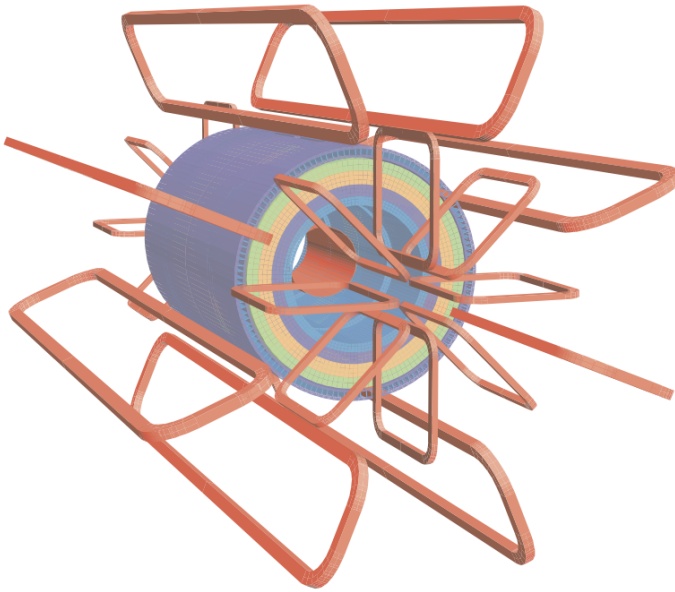


Figure 3.9: Layout of the barrel and endcap toroid magnets [13]

430 3.6 Forward Detectors

431 In addition to the inner detector, calorimeters, and muon spectrometer, three smaller detectors
 432 provide coverage in the very forward region. The innermost forward detector, at 17 m from the
 433 interaction point, is the **L**Uminosity measurement using **C**erenkov **I**ntegrating **D**etector (LUCID).
 434 LUCID's primary purpose is to measure the relative online-luminosity for the ATLAS detector,
 435 from inelastic $p - p$ scattering. The detector is composed of 20 aluminum Cerenkov tubes which
 436 surround the beam pipe and face towards the interaction point.

437 The second forward detector is the Zero-Degree Calorimeter (ZDC), located 140 m from the
 438 interaction point in both directions, at the point where the LHC beam-pipe divides into two separate
 439 pipes. The ZDC's primary purpose is to detect forward neutrons from heavy ion collisions.

440 The third forward detector is the Absolute Luminosity For ATLAS (ALFA) system, located 240
 441 m from the interaction point in both directions. ALFA determines luminosity by measuring elastic
 442 scattering at small angles, from which luminosity can be calculated via the optical theorem. The
 443 detector is built from scintillating fiber trackers. These are connected to the accelerator vacuum

444 via Roman pots, which allow the detector to come as close as 1mm to the beam without disrupting
445 the machine vacuum. The LUCID and ALFA detectors are crucial to determining the real-time
446 conditions of the beams and the total luminosity delivered to the ATLAS detector [13].

447 **3.7 Trigger and Data Acquisition**

448 The trigger and Data Acquisition systems (TDAQ) are responsible for selecting the most viable
449 events to save for further downstream processing. Because of the high luminosities delivered to
450 the ATLAS detector, not all events recorded can be saved; the 40 MHz bunch crossing rate must
451 be reduced by 5 orders of magnitude to an event storage rate of \sim 1 kHz. The trigger system is
452 composed of three distinct levels: Level 1 (L1), Level 2 (L2) and the event filter. Collectively the
453 L2 trigger and the event filter form the High Level Trigger (HLT).

454 The L1 trigger is implemented in the hardware of the ATLAS calorimeter and muon systems.
455 The primary modality of the L1 trigger is to identify muons, electrons, photons, jets, and τ -leptons
456 with high transverse momentum. Particles with high transverse momentum are more likely to
457 originate from direct, high energy collisions, which are most likely to produce interesting physics
458 processes. The L1 trigger also identifies events with large missing transverse energy, which could
459 be indicative of new physics. The L1 muon trigger (L1Muon) relies on RPC and TGC trigger
460 chambers in the barrel and end-cap regions of the muon spectrometer. The L1 Calorimeter Trigger
461 (L1Calo) uses reduced granularity information collected by all the calorimeter subsystems. Results
462 from the L1Muon and L1Calo triggers are combined by the Central Trigger Processor (CTP),
463 which implements a trigger ‘menu’, listing various combinations of trigger requirements. The
464 maximum L1 acceptance rate is 75 kHz, and the L1 trigger decision must reach the front-end
465 electronics within $2.5 \mu\text{s}$ of it’s associated bunch-crossing [13].

466 The L1 trigger defines a Region-of-Interest (RoI) for each passing event. The ROI is repre-
467 sented by the η - ϕ detector region where interesting features were identified by the L1 selection
468 process. Information about the type of feature identified and the threshold which was exceeded to
469 trigger the L1 response is also recorded. The ROI data is sent to the L2 trigger, which uses all of

470 the available information within the ROI at full granularity and precision. The L2 trigger reduces
471 the event rate from 75 kHz to 3.5 kHz, with an average processing time of 40 ms. The final stage of
472 the HLT is the event filter, which reduces the event rate to 200 Hz. The event filter uses an offline
473 analysis process to select fully rebuilt events which will be saved for further analysis.

474 All levels of the ATLAS trigger system depend on specialized electronics. Each detector front-
475 end system has a specialized Readout Driver (ROD) which collects information from several front-
476 end data streams at once. The ROD is composed of front-end analogue processing, an L1 buffer
477 which retains the information long enough for the L1 trigger decision, and dedicated links which
478 send the front-end L1 triggered data to Data Acquisition System (DAQ). Any digital signals are
479 formatted as raw data before being transferred to the DAQ. The first stage of the DAQ temporarily
480 stores the L1 data in local buffers. The ROI data is then requested by the L2 trigger, after which
481 selected events are transferred to an event building system, before events passing the event filter
482 are sent to the CERN computer center for permanent storage. The DAQ system not only allows
483 for the readout of detector data, but is also responsible for the monitoring and configuration of
484 the hardware and software components which make up the data readout system via the Detector
485 Control System (DCS).

486 The DCS allows centralized control of all detector subsystems simultaneously. It continually
487 monitors operational conditions, reports any abnormal behavior to the operator, and can perform
488 both automatic and manual interventions. The DCS reports on real time detector conditions such
489 as high or low voltage detector electronics, gas and cooling systems, magnetic field conditions,
490 humidity and temperature. This information is continually monitored by experts in the ATLAS
491 control room, so that action can be taken immediately to correct any issues that arise. The DCS also
492 handles communication between detector systems, and other systems such as the LHC accelerator,
493 the ATLAS magnets, and CERN technical services [13].

Chapter 4: Particle Reconstruction and Identification

496 Lorem ipsum dolor sit amet, consectetur adipiscing elit, sed do eiusmod tempor incididunt ut
497 labore et dolore magna aliqua. Ut enim ad minim veniam, quis nostrud exercitation ullamco laboris
498 nisi ut aliquip ex ea commodo consequat. Duis aute irure dolor in reprehenderit in voluptate velit
499 esse cillum dolore eu fugiat nulla pariatur. Excepteur sint occaecat cupidatat non proident, sunt in
500 culpa qui officia deserunt mollit anim id est laborum.. Lorem ipsum dolor sit amet, consectetur
501 adipiscing elit, sed do eiusmod tempor incididunt ut labore et dolore magna aliqua. Ut enim ad
502 minim veniam, quis nostrud exercitation ullamco laboris nisi ut aliquip ex ea commodo consequat.
503 Duis aute irure dolor in reprehenderit in voluptate velit esse cillum dolore eu fugiat nulla pariatur.
504 Excepteur sint occaecat cupidatat non proident, sunt in culpa qui officia deserunt mollit anim id est
505 laborum..

Conclusion or Epilogue

507 Use this page for your epilogue or conclusion if applicable; please use only one of the titles
508 for this page. Otherwise, you may delete it. Use this page for your epilogue or conclusion if
509 applicable; please use only one of the titles for this page. Otherwise, you may delete it. Use this
510 page for your epilogue or conclusion if applicable; please use only one of the titles for this page.
511 Otherwise, you may delete it. Use this page for your epilogue or conclusion if applicable; please
512 use only one of the titles for this page. Otherwise, you may delete it. Use this page for your
513 epilogue or conclusion if applicable; please use only one of the titles for this page. Otherwise,
514 you may delete it. Use this page for your epilogue or conclusion if applicable; please use only one
515 of the titles for this page. Otherwise, you may delete it. Use this page for your epilogue or
516 conclusion if applicable; please use only one of the titles for this page. Otherwise, you may delete
517 it. Use this page for your epilogue or conclusion if applicable; please use only one of the titles for
518 this page. Otherwise, you may delete it. Use this page for your epilogue or conclusion if
519 applicable; please use only one of the titles for this page. Otherwise, you may delete it. Use this
520 page for your epilogue or conclusion if applicable; please use only one of the titles for this page.
521 Otherwise, you may delete it. Use this page for your epilogue or conclusion if applicable; please
522 use only one of the titles for this page. Otherwise, you may delete it. Use this page for your
523 epilogue or conclusion if applicable; please use only one of the titles for this page. Otherwise,
524 you may delete it. Use this page for your epilogue or conclusion if applicable; please use only one
525 of the titles for this page. Otherwise, you may delete it. Use this page for your epilogue or
526 conclusion if applicable; please use only one of the titles for this page. Otherwise, you may delete

527 it. Use this page for your epilogue or conclusion if applicable; please use only one of the titles for
528 this page. Otherwise, you may delete it. Use this page for your epilogue or conclusion if
529 applicable; please use only one of the titles for this page. Otherwise, you may delete it. Use this
530 page for your epilogue or conclusion if applicable; please use only one of the titles for this page.
531 Otherwise, you may delete it. Use this page for your epilogue or conclusion if applicable; please
532 use only one of the titles for this page. Otherwise, you may delete it. Use this page for your
533 epilogue or conclusion if applicable; please use only one of the titles for this page. Otherwise,
534 you may delete it. Use this page for your epilogue or conclusion if applicable; please use only one
535 of the titles for this page. Otherwise, you may delete it. Use this page for your epilogue or
536 conclusion if applicable; please use only one of the titles for this page. Otherwise, you may delete
537 it. Use this page for your epilogue or conclusion if applicable; please use only one of the titles for
538 this page. Otherwise, you may delete it. Use this page for your epilogue or conclusion if
539 applicable; please use only one of the titles for this page. Otherwise, you may delete it. Use this
540 page for your epilogue or conclusion if applicable; please use only one of the titles for this page.
541 Otherwise, you may delete it. Use this page for your epilogue or conclusion if applicable; please
542 use only one of the titles for this page. Otherwise, you may delete it. Use this page for your
543 epilogue or conclusion if applicable; please use only one of the titles for this page. Otherwise,
544 you may delete it. Use this page for your epilogue or conclusion if applicable; please use only one
545 of the titles for this page. Otherwise, you may delete it. Use this page for your epilogue or
546 conclusion if applicable; please use only one of the titles for this page. Otherwise, you may delete
547 it. Use this page for your epilogue or conclusion if applicable; please use only one of the titles for
548 this page. Otherwise, you may delete it. Use this page for your epilogue or conclusion if
549 applicable; please use only one of the titles for this page. Otherwise, you may delete it. Use this
550 page for your epilogue or conclusion if applicable; please use only one of the titles for this page.
551 Otherwise, you may delete it. Use this page for your epilogue or conclusion if applicable; please
552 use only one of the titles for this page. Otherwise, you may delete it. Use this page for your
553 epilogue or conclusion if applicable; please use only one of the titles for this page. Otherwise,

554 you may delete it. Use this page for your epilogue or conclusion if applicable; please use only one
555 of the titles for this page. Otherwise, you may delete it. Use this page for your epilogue or
556 conclusion if applicable; please use only one of the titles for this page. Otherwise, you may delete
557 it. Use this page for your epilogue or conclusion if applicable; please use only one of the titles for
558 this page. Otherwise, you may delete it. Use this page for your epilogue or conclusion if
559 applicable; please use only one of the titles for this page. Otherwise, you may delete it. Use this
560 page for your epilogue or conclusion if applicable; please use only one of the titles for this page.
561 Otherwise, you may delete it. Use this page for your epilogue or conclusion if applicable; please
562 use only one of the titles for this page. Otherwise, you may delete it. Use this page for your
563 epilogue or conclusion if applicable; please use only one of the titles for this page. Otherwise,
564 you may delete it. Use this page for your epilogue or conclusion if applicable; please use only one
565 of the titles for this page. Otherwise, you may delete it. Use this page for your epilogue or
566 conclusion if applicable; please use only one of the titles for this page. Otherwise, you may delete
567 it. Use this page for your epilogue or conclusion if applicable; please use only one of the titles for
568 this page. Otherwise, you may delete it. Use this page for your epilogue or conclusion if
569 applicable; please use only one of the titles for this page. Otherwise, you may delete it. Use this
570 page for your epilogue or conclusion if applicable; please use only one of the titles for this page.
571 Otherwise, you may delete it. Use this page for your epilogue or conclusion if applicable; please
572 use only one of the titles for this page. Otherwise, you may delete it. Use this page for your
573 epilogue or conclusion if applicable; please use only one of the titles for this page. Otherwise,
574 you may delete it. Use this page for your epilogue or conclusion if applicable; please use only one
575 of the titles for this page. Otherwise, you may delete it. Use this page for your epilogue or
576 conclusion if applicable; please use only one of the titles for this page. Otherwise, you may delete
577 it. Use this page for your epilogue or conclusion if applicable; please use only one of the titles for
578 this page. Otherwise, you may delete it. Use this page for your epilogue or conclusion if
579 applicable; please use only one of the titles for this page. Otherwise, you may delete it. Use this
580 page for your epilogue or conclusion if applicable; please use only one of the titles for this page.

581 Otherwise, you may delete it. Use this page for your epilogue or conclusion if applicable; please
582 use only one of the titles for this page. Otherwise, you may delete it. Use this page for your
583 epilogue or conclusion if applicable; please use only one of the titles for this page. Otherwise,
584 you may delete it. Use this page for your epilogue or conclusion if applicable; please use only one
585 of the titles for this page. Otherwise, you may delete it. Use this page for your epilogue or
586 conclusion if applicable; please use only one of the titles for this page. Otherwise, you may delete
587 it. Use this page for your epilogue or conclusion if applicable; please use only one of the titles for
588 this page. Otherwise, you may delete it. Use this page for your epilogue or conclusion if
589 applicable; please use only one of the titles for this page. Otherwise, you may delete it. Use this
590 page for your epilogue or conclusion if applicable; please use only one of the titles for this page.
591 Otherwise, you may delete it. Use this page for your epilogue or conclusion if applicable; please
592 use only one of the titles for this page. Otherwise, you may delete it. Use this page for your
593 epilogue or conclusion if applicable; please use only one of the titles for this page. Otherwise,
594 you may delete it. Use this page for your epilogue or conclusion if applicable; please use only one
595 of the titles for this page. Otherwise, you may delete it. Use this page for your epilogue or
596 conclusion if applicable; please use only one of the titles for this page. Otherwise, you may delete
597 it. Use this page for your epilogue or conclusion if applicable; please use only one of the titles for
598 this page. Otherwise, you may delete it. Use this page for your epilogue or conclusion if
599 applicable; please use only one of the titles for this page. Otherwise, you may delete it. Use this
600 page for your epilogue or conclusion if applicable; please use only one of the titles for this page.
601 Otherwise, you may delete it. Use this page for your epilogue or conclusion if applicable; please
602 use only one of the titles for this page. Otherwise, you may delete it. Use this page for your
603 epilogue or conclusion if applicable; please use only one of the titles for this page. Otherwise,
604 you may delete it. Use this page for your epilogue or conclusion if applicable; please use only one
605 of the titles for this page. Otherwise, you may delete it. Use this page for your epilogue or
606 conclusion if applicable; please use only one of the titles for this page. Otherwise, you may delete
607 it.

References

- [1] M. Tanabashi et al. “Review of Particle Physics”. In: *Phys. Rev. D* 98 (3 2018), pp. 847–851.
- [2] Lyndon Evans and Philip Bryant. “LHC Machine”. In: *Journal of Instrumentation* 3.08 (2008), S08001.
- [3] “The ATLAS Experiment at the CERN Large Hadron Collider”. In: *JINST* 3 (2008). Also published by CERN Geneva in 2010, S08003.
- [4] “The CMS experiment at the CERN LHC”. In: *Journal of Instrumentation* 3.08 (2008), S08004.
- [5] “The ALICE experiment at the CERN LHC”. In: *Journal of Instrumentation* 3.08 (2008), S08002.
- [6] “The LHCb Detector at the LHC”. In: *Journal of Instrumentation* 3.08 (2008), S08005.
- [7] Ana Lopes and Melissa Loyse Perrey. *FAQ-LHC The guide*. 2022.
- [8] Esma Mobs. “The CERN accelerator complex in 2019. Complexe des accélérateurs du CERN en 2019”. In: (2019). General Photo.
- [9] *Pulling together: Super Conducting electromagnets*. <https://home.cern/science/engineering/pulling-together-superconducting-electromagnets>. Accessed: 2024-01-05.
- [10] *The High-Luminosity LHC*. <https://voisins.web.cern.ch/en/high-luminosity-lhc-hl-lhc>. Accessed: 2024-01-05.
- [11] Aad G., et al. (ATLAS Collaboration and CMS Collaboration). “Combined Measurement of the Higgs Boson Mass in pp Collisions at $\sqrt{s} = 7$ and 8 TeV with the ATLAS and CMS Experiments”. In: *Phys. Rev. Lett.* 114 (19 2015), p. 191803.
- [12] O. Aberle et al. *High-Luminosity Large Hadron Collider (HL-LHC): Technical design report*. CERN Yellow Reports: Monographs. Geneva: CERN, 2020.
- [13] The ATLAS Collaboration. “The ATLAS Experiment at the CERN Large Hadron Collider”. In: *Journal of Instrumentation* 3.08 (2008), S08003.

- 634 [14] G Aad, B Abbott, and ATLAS Collaboration. “Performance of the reconstruction of large
635 impact parameter tracks in the inner detector of ATLAS”. In: *Eur. Phys. J. C Part. Fields*
636 83.11 (Nov. 2023).
- 637 [15] Joao Pequenao. *Computer Generated image of the ATLAS calorimeter*. 2008.
- 638 [16] *ATLAS liquid-argon calorimeter: Technical Design Report*. Technical design report. AT-
639 LAS. Geneva: CERN, 1996.
- 640 [17] H A Gordon. “Liquid argon calorimetry for the SSC”. In: () .
- 641 [18] Henric Wilkens and (on behalf ofthe ATLAS LArg Collaboration). “The ATLAS Liquid
642 Argon calorimeter: An overview”. In: *Journal of Physics: Conference Series* 160.1 (2009),
643 p. 012043.
- 644 [19] *Technical Design Report for the Phase-II Upgrade of the ATLAS Tile Calorimeter*. Tech.
645 rep. Geneva: CERN, 2017.
- 646 [20] “Technical Design Report for the Phase-II Upgrade of the ATLAS Muon Spectrometer”. In:
647 () .
- 648 [21] L Pontecorvo. “The ATLAS Muon Spectrometer”. In: (2004). revised version number 1
649 submitted on 2003-07-27 16:31:16.
- 650 [22] *ATLAS magnet system: Technical Design Report, 1*. Technical design report. ATLAS. Geneva:
651 CERN, 1997.

652

653

Appendix A: Experimental Equipment

654 Lorem ipsum dolor sit amet, consectetur adipiscing elit, sed do eiusmod tempor incididunt ut
655 labore et dolore magna aliqua. Ut enim ad minim veniam, quis nostrud exercitation ullamco laboris
656 nisi ut aliquip ex ea commodo consequat. Duis aute irure dolor in reprehenderit in voluptate velit
657 esse cillum dolore eu fugiat nulla pariatur. Excepteur sint occaecat cupidatat non proident, sunt in
658 culpa qui officia deserunt mollit anim id est laborum.

659

660

Appendix B: Data Processing

661 Lorem ipsum dolor sit amet, consectetur adipiscing elit, sed do eiusmod tempor incididunt ut
662 labore et dolore magna aliqua. Ut enim ad minim veniam, quis nostrud exercitation ullamco laboris
663 nisi ut aliquip ex ea commodo consequat. Duis aute irure dolor in reprehenderit in voluptate velit
664 esse cillum dolore eu fugiat nulla pariatur. Excepteur sint occaecat cupidatat non proident, sunt in
665 culpa qui officia deserunt mollit anim id est laborum.